

Partial photoionization cross sections for Hg between 600 and 250 Å. Effect of spin-orbit coupling on the ${}^2D_{5/2}/{}^2D_{3/2}$ branching ratio of Hg^{\dagger}

J. L. Dehmer and J. Berkowitz

Argonne National Laboratory, Argonne, Illinois 60439

(Received 25 March 1974)

By means of photoelectron spectroscopy, we have measured the branching ratios for production of the ${}^2S_{1/2}$, ${}^2D_{5/2}$, and ${}^2D_{3/2}$ states of Hg^{\dagger} by photoionization of Hg in the wavelength range 600–250 Å. These branching ratios are combined with earlier measurements of the total photoionization cross section to produce partial photoionization cross sections for the above processes. The wavelength dependence of the ${}^2D_{5/2}:{}^2D_{3/2}$ branching ratio exhibits a systematic deviation relative to the statistical value of 3:2. That is, this ratio is greater than statistical where the respective partial cross sections are increasing with photon energy and is less than statistical when the partial cross sections are decreasing. This effect was previously predicted and is a consequence of spin-orbit coupling in the ionized subshell, in this case, the 5*d* subshell of Hg.

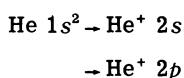
I. INTRODUCTION

Photoabsorption by an atom or molecule in the spectral range above the second photoionization threshold leads to the competitive production of alternative final ionic states. At each wavelength, the relative frequencies with which different ionic states are formed are denoted by a set of branching ratios. In the case of the present study, photoabsorption by gaseous mercury in the wavelength range $600 \text{ \AA} \geq \lambda \geq 250 \text{ \AA}$ leads to the ionic states $5d^{10}6s\ {}^2S_{1/2}$, $5d^96s^2\ {}^2D_{5/2}$, and $5d^96s^2\ {}^2D_{3/2}$ of Hg^{\dagger} (states of Hg^{\dagger} having other configurations, such as $5d^{10}6p$, are also produced with much smaller probability and will be treated separately¹). Photoionization branching ratios are best determined by means of photoelectron spectroscopy. Since the formation of alternative ionic states produces photoelectrons with different kinetic energies, the relative areas under the peaks in a photoelectron spectrum may be considered the raw data for the branching ratios. True branching ratios are derived by taking into account the effects of photoelectron angular distributions and the spectrometer transmission function, both of which depend upon the particular experimental arrangement. When a complete set of branching ratios is known, together with the absolute total photoionization cross section, one can determine the *partial* photoionization cross sections for each ionization channel. Such partial photoionization cross sections are functions of the wavelength of the incident radiation so that it is necessary, in general, to measure the branching ratios as a function of wavelength. We have been able to characterize the rather smooth variation of the Hg branching ratios by using four conveniently spaced wavelengths: 584 Å (He I), 461.5 Å (Ne II), 304 Å and 256 Å (He II).

The present study on Hg was motivated by a recent prediction by Walker *et al.*² to the effect that the ${}^2D_{5/2}:{}^2D_{3/2}$ branching ratio would be larger than the statistical value of 3:2 when the partial cross sections for these channels are increasing with photon energy, and would be smaller than statistical when the partial cross sections are falling. This effect derives from the spin-orbit coupling in the 5*d* subshell, and was calculated using the Dirac-Slater model.³ At the time of the calculation, only fragmentary data were available to support this interpretation: At 584 Å the partial cross sections for ionization from the outer *np* subshell of Ar, Kr, and Xe are known⁴ to be falling with increasing $\hbar\omega$. Hence, the ${}^2P_{3/2}:{}^2P_{1/2}$ branching ratios at 584 Å would be predicted to be smaller than the statistical value of 2:1, which they are.⁵ Examples of larger-than-statistical branching ratios were provided² by the ${}^2D_{5/2}:{}^2D_{3/2}$ ratios of Zn, Cd, and Hg at 584 Å. These data motivated and supported the arguments of Walker *et al.*; but at that time no wavelength-dependent data were known for a subshell with resolvable spin-orbit splitting which illustrated the “cross-over” from above to below the statistical value which would be observed upon passing through a maximum in the partial cross section of the subshells. Mercury is a convenient candidate for illustration of this crossover since the 5*d* subshell has large spin-orbit splitting (which causes the effect to be more pronounced), and the maximum in its partial cross section lies in the range of available light sources.

Only a small number of studies of the wavelength dependence of atomic branching ratios have been reported. Comes and Sälzer⁶ and Samson and Cairns⁵ have reported the wavelength dependence of the ${}^2P_{3/2}:{}^2P_{1/2}$ branching ratios for the rare gases. We have already used the values of

these ratios at 584 Å as examples of nonstatistical behavior. However, it should also be possible to observe variations in this ratio in the wavelength region studied. Samson and Cairns report a constant value within the error of the counting statistics. Comes and Sälzer report a flat variation with wavelength except near the $^2P_{1/2}$ threshold in Ar and Kr where the $^2P_{3/2}:^2P_{1/2}$ ratio increases above the statistical value of 2:1. This may be significant, since for Ar and Kr the ionization cross sections are rising there. However, the situation should be reexamined experimentally. More recently Krause and Wuilleumier⁷ have measured the branching ratio for the processes



as a function of wavelength. Also, Wuilleumier and Krause⁸ have measured partial photoionization cross sections for Ne in the wavelength range $100 \leq \hbar\omega \leq 2000$ eV. However, neither of these latter experiments permit testing of the effect of spin-orbit splitting discussed above.

In the case of molecules, NO,⁹⁻¹¹ N₂O,¹⁰ CO,¹⁰ CO₂,^{10,12,13} NH₃,¹⁰ I₂,¹⁴ Br₂,¹⁴ and O₂¹⁵ have been studied. It is interesting to note that the $^2\Pi_{3/2,g} : ^2\Pi_{1/2,g}$ branching ratio for I₂ also manifests significant deviation from the corresponding ratio of 1:1 for $\lambda < 900$ Å. This effect, also attributable in part to the spin-orbit effect in the iodine $5p\pi$ orbitals, has not been analyzed in detail.

II. EXPERIMENTAL DETAILS

In this experiment, undispersed radiation from a hollow-cathode discharge lamp (HCL) is crossed

with a mercury beam in the source region of a cylindrical-mirror electron energy analyzer (CMA). A schematic diagram of the apparatus is given in Fig. 1.

Details of the design and construction of the CMA have been given elsewhere¹⁶; however, two characteristics bear directly on quantitative measurement of branching ratios and warrant special comment. First, the photoelectrons are dispersed in the intercylinder region at their original ejection energy. Since the resolving power of the analyzer is constant, $\Delta E/E \cong 0.8\%$, the resolution varies across the spectrum, remaining proportional to the kinetic energy. This has the effect of enhancing the total area under a photoelectron peak at high kinetic energy relative to one at lower kinetic energy. Hence, relative photoelectron intensities are deduced by dividing the area of photoelectron peaks by the corresponding kinetic energy. (Below ~1-eV kinetic energy the spectrometer transmission function falls off, introducing another correction, but this situation does not arise in this experiment.) Second, the entrance slit of the CMA accepts electrons ejected at an angle of 60° relative to the direction of the unpolarized light beam. Hence, we are measuring intensities which are proportional to the differential cross section, given by

$$\frac{d\sigma_i^{60^\circ}(E)}{d\Omega} = \frac{\sigma_i^T(E)}{4\pi} \left[1 - \frac{1}{2}\beta_i(E)P_2(\cos 60^\circ) \right], \quad (1)$$

where the subscript i denotes ionization from a particular atomic orbital, and the argument E is included to denote quantities which depend on the energy of the ionizing radiation. Since the present analyzer is not set at the "magic angle" of 54°44'

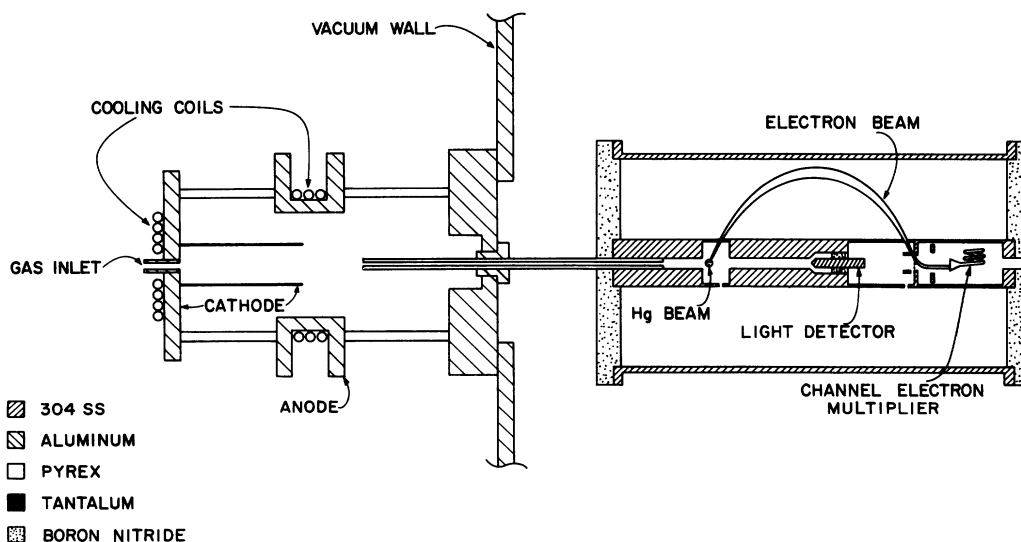


FIG. 1. Schematic diagram of experimental apparatus.

[for which $P_2(\cos\theta)=0$], the effect of photoelectron angular distribution must be taken into account in order to determine the branching ratio for a given pair of ionization processes, given by $\sigma_i^T(E)/\sigma_j^T(E)$. In the present case this quantity is related to the measured quantity by

$$\frac{\sigma_i^T(E)}{\sigma_j^T(E)} = \frac{[1 - 0.0625\beta_i(E)]}{[1 - 0.0625\beta_j(E)]} \frac{d\sigma_i^{90^\circ}(E)/d\Omega}{d\sigma_j^{90^\circ}(E)/d\Omega}. \quad (2)$$

The HCL illustrated in Fig. 1 was patterned after one described by Newburgh *et al.*¹⁷ Some of its performance characteristics have been previously described.¹⁸ The anode and back plate are made of aluminum, are water cooled, and are separated by sections of thick-walled Pyrex tubing. Vacuum seals are made with Viton "O-rings," and the assembly is clamped with insulated bolts (not shown) connecting the back plate with the anode section and the anode section with the mounting flange. The hollow cathode is made of 0.020-in. tantalum tubing which is covered by a close-fitting quartz tube (not shown). The lamp was typically operated with 0.4-A discharge current and cathode voltages between -500 and -1000 V, depending upon the gas and its pressure. Typical pressures used were 1 Torr He for 584 Å, 0.3 Torr He for 304 Å, and 0.2 Torr 90% Ne-10% He for 461.5 Å. The He II/He I ratio varied from ~0.09 at 1 Torr to ~0.18 at 0.2 Torr. Absolute intensities were not measured, but are believed to be in the range of 10^{10} photons $\text{sec}^{-1} \text{mm}^{-2}$ in the collision region.

A section of 2-mm-bore capillary tubing was used to channel the output of the HCL into the ionization region. This detail was essential to the feasibility of the experiment, providing an enhancement of approximately three orders of

magnitude in counting rate. Typical counting rates for the $^2D_{5/2}$ state of Hg^+ were $\sim 20 \times 10^3$ counts/sec at 584 Å and $\sim 5 \times 10^3$ counts/sec at 304 Å.

III. RESULTS

Figure 2 illustrates typical spectra of the $^2D_{3/2}$ and $^2D_{5/2}$ peaks formed by 584- and 304-Å radiation, respectively. These spectra were recorded at 1 channel/sec and were juxtaposed by changing the energy scale in the middle of the scan in order to compare the ratio of the 584- and 304-Å lines under the same source and lamp conditions. However, aside from indicating the ratio of light output discussed in Sec. IV, this spectrum serves to illustrate two other points. First, the 304-Å peaks are several times broader than the 584-Å peaks. This effect was mentioned in Sec. II and reflects the fact that the resolution is proportional to the kinetic energy in the present mode of operation (which does not retard the photoelectrons before they are energy analyzed). This effect does not hinder the present measurements since all the accessible ionic states of Hg^+ are easily resolved and the broadening can be taken into account merely by dividing the area of the peak by the kinetic energy of the ejected electrons. Moreover, the absence of electron lenses or retarding grids has the advantage of a less complicated transmission function which is well characterized. Second, the more important aspect illustrated in Fig. 2 is the rather large difference in relative peak heights between the two sets of peaks. That is, at 584 Å the $^2D_{5/2}$ state is formed more than twice as often as the $^2D_{3/2}$ state, whereas at 304 Å the probabilities are roughly comparable. Hence, with these

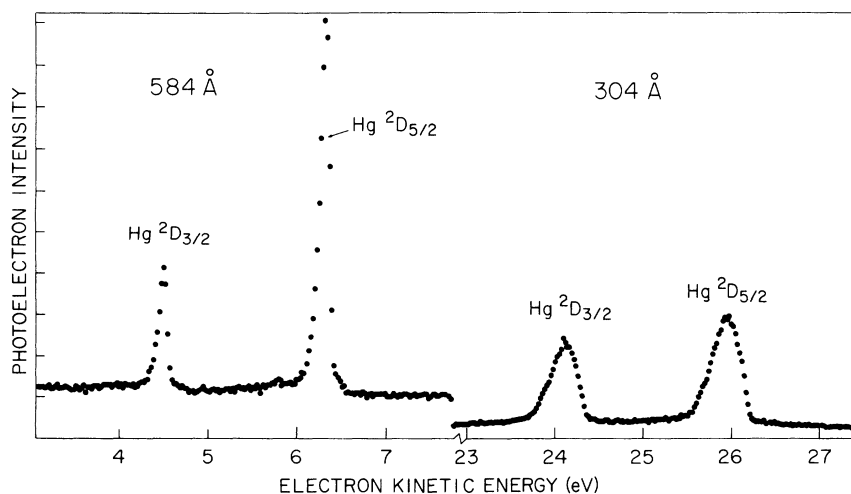


FIG. 2. Comparison of the mercury $^2D_{3/2}$ and $^2D_{5/2}$ photoelectron peaks taken with 584- and 304-Å radiation.

two spectra alone, we already see ${}^2D_{5/2}:{}^2D_{3/2}$ ratios which are above and below the statistical value of 3:2.

An effect which must always be considered in measuring branching ratios is that of the scattering of photoelectrons from the background gas in the analyzer. This is particularly acute in the 584-Å spectrum of Hg. In this spectrum, electrons with kinetic energies of 4.513 eV (${}^2D_{3/2}$), 6.377 eV (${}^2D_{5/2}$) and 10.780 eV (${}^2S_{1/2}$) are produced which have total scattering cross sections on mercury¹⁹ of $\sim 3.6 \times 10^{-15}$ cm², $\sim 2.5 \times 10^{-15}$ cm², and $\sim 1.2 \times 10^{-15}$ cm², respectively. Hence, there can be strong attenuation of the photoelectrons in the selected beam at modest pressures. Moreover, the scattering will attenuate the slower electrons more than the more energetic ones, and this will distort the observed peak intensities relative to the true branching ratio. The necessary precaution is to measure the spectra at several pressures and extrapolate to zero pressure. A series of measurements of this type is shown in Fig. 3 for the ${}^2D_{5/2}:{}^2D_{3/2}$ and ${}^2D_{5/2}:{}^2S_{1/2}$ ratios at 584 Å. Here each point represents the average of several measurements, and the intercept at $P=0$ is still uncorrected for the effects of photoelectron angular distributions (see below). The measurements were conducted as a function of background pressure in the vacuum chamber (which is assumed to be proportional to the pressure in the source region). At shorter wavelengths, this problem is much less severe because of smaller magnitudes and differences in magnitude of total scattering cross sections for the different photoelectrons. Hence, these measurements were conducted at moderate background pressures, and no pressure-dependence test was conducted.

Our experimental results are summarized in Table I. The wavelength of the radiation, the term value for the final ionic states, and the

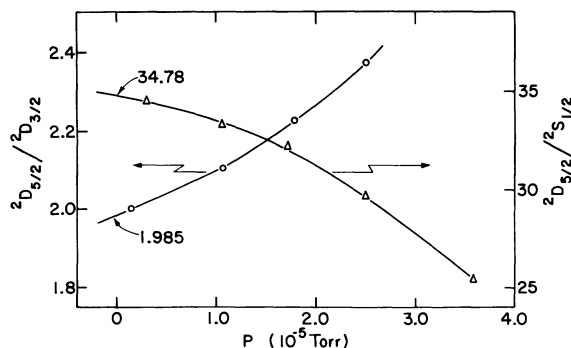


FIG. 3. Pressure dependence of the ${}^2D_{5/2}:{}^2D_{3/2}$ and ${}^2D_{5/2}:{}^2S_{1/2}$ branching ratios for mercury. Pressure scale denotes background pressure in the vacuum chamber.

corresponding photoelectron kinetic energies are given in the first three columns. The fourth column lists the asymmetry parameters used for the correction in Eq. (2). These were obtained by using atomic wave functions obtained from Hartree-Slater atomic potentials²⁰ and the Cooper-Zare formula²¹ which expresses β in pure LS coupling. The differences in β for the electrons associated with a ${}^2D_{5/2}$ and ${}^2D_{3/2}$ state are due purely to the difference in kinetic energy. Manson²² found this approximate scheme to yield satisfactory agreement with experiment for photoionization of Hg at 584 Å. The next two columns contain the raw (60°) branching ratios and those corrected for angular distribution effects. The correction for the ${}^2D_{5/2}:{}^2D_{3/2}$ ratio was a few percent owing to the similarity between the respective values of β . The ${}^2D_{5/2}:{}^2S_{1/2}$ correction was larger, $\sim 11\%$, and is a consequence of the extreme value $\beta=2$ characteristic for the ionization of an electron from an s orbital.

The last column of Table I lists the 584-Å results of Frost *et al.*²³ Notice that the deviation from our

TABLE I. Experimental branching ratios for Hg.

λ (Å)	Kinetic energy (eV)	β	60° data	Branching ratio	From Ref. 23	
584	${}^2S_{1/2}$	10.780	2.000	0.0288	0.0252	0.0671
	${}^2D_{5/2}$	6.377	-0.250	1.000	1.000	1.000
	${}^2D_{3/2}$	4.513	-0.117	0.504	0.499	0.419
461	${}^2D_{5/2}$	12.022	-0.102	1.000	1.000	...
	${}^2D_{3/2}$	10.158	-0.189	0.617	0.621	...
304	${}^2S_{1/2}$	30.375	2.000	0.0288	0.0265	...
	${}^2D_{5/2}$	25.972	0.545	1.000	1.000	...
	${}^2D_{3/2}$	24.108	0.473	0.725	0.728	...
256	${}^2D_{5/2}$	33.530	0.803	1.000	1.000	...
	${}^2D_{3/2}$	31.666	0.744	0.758	0.760	...

results is in the same direction as the pressure effect shown in Fig. 3. In their experiment, Frost *et al.* operate at a background pressure of 10^{-2} Torr in their spherical retarding analyzer. Although in principle this type of analyzer collects all ejected electrons, it may be possible that electrons impinging upon the tubes used to introduce and collect the radiation were collected there and thus not detected. The fraction of the electrons of a particular kinetic energy so collected would, of course, be proportional to the total scattering cross section for that kinetic energy. Thus, it is possible that the measurements of Frost *et al.* would exhibit a similar pressure effect to that shown in Fig. 3 that was not taken into account. In an earlier publication, Frost *et al.*²⁴ stated, "At or below this pressure (10^{-4} Torr for Ar) we found no dependence on pressure of the relative heights of the photoelectron 'steps' in a spectrum." If, indeed, a pressure effect was observed at the upper limit in this case, then a pressure effect in the mercury measurement is most likely.

The wavelength dependence of the ${}^2D_{5/2} : {}^2D_{3/2}$ branching ratio was determined for the range $600 \text{ \AA} \geq \lambda \geq 200 \text{ \AA}$ by constructing a smooth curve through the points from Table I. This is shown in Fig. 4. A marked variation relative to the statistical value is evident, with a crossover at $\lambda \sim 400 \text{ \AA}$. This is discussed in Sec. IV.

It is possible to convert the branching-ratio data in Table I into partial cross sections by using the relative total photoionization data of Cairns *et al.*²⁵ (which covers the range $10 \leq \hbar\omega \leq 70$ eV) together with the absolute photoabsorption cross section of the $5d^{10}6s^2 {}^1S_0 - 5d^9 6s^2 6p {}^3P_1$ transition reported by Lincke and Stredele.²⁶ Originally, Cairns *et al.* had adopted an oscillator strength of 0.77 for this transition based on the electron impact work of Skerbele *et al.*²⁷ However, the absolute optical oscillator strength of this transition has recently been reported to be 0.53 by Lincke and Stredele,²⁶ which implies that the

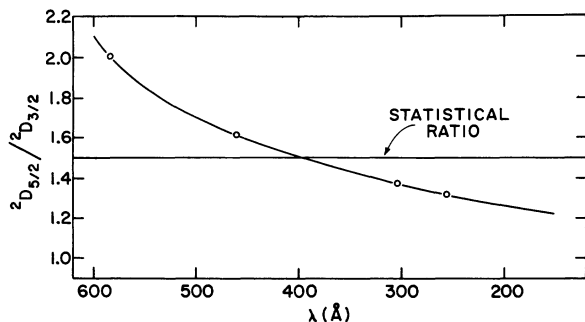


FIG. 4. Wavelength dependence of ${}^2D_{5/2} : {}^2D_{3/2}$ branching ratio for mercury.

data of Cairns *et al.* can be put on an absolute scale by renormalizing their data by a factor of $\frac{0.53}{0.77} = 0.69$. With the intention of checking the consistency of data from different laboratories, we have also normalized the relative photoionization cross section of Berkowitz and Lifshitz²⁸ to the Lincke and Stredele measurement. Comparison of these normalized data with those of Cairns *et al.* implies that a correction factor of ~ 0.5 must be used to renormalize the latter. To resolve this dilemma, the tabulated data of Cairns *et al.* were integrated between 16.8 and 72 eV (including the Hg^{++} contribution), yielding an f value of 18.56. This number includes about a 10% contribution from Hg^{++} and a much smaller contribution from the $6s$ shell, but fails to span the full spectral range of the $5d$ -shell contribution. Even in view of these qualifications, it is clear that the f value of ~ 19 greatly exceeds the f value of ~ 10 which is expected. (Although the Thomas-Reiche-Kuhn sum rule cannot be applied rigorously on a subshell basis, it can be used with confidence at the level of this comparison).

In addition, the $S(-1)$ and $S(-2)$ sum rules, though less sensitive to cross sections in the 16.8–72 eV region, also support the conclusion that the approximate cross sections of Cairns *et al.* are about a factor of 2 too high.²⁹ All of these considerations tend to support the second estimate above. Therefore, we have chosen to scale the data of Cairns *et al.* by 0.5. This should provide $\pm 30\%$ accuracy, in any case.

We applied this choice of normalization to a smooth fit to the data of Cairns *et al.*, resulting in the dashed curve in Fig. 5. The full set of partial-cross-section curves was then prepared in the following steps. First, the "absolute" total ionization cross section at 584 and 304 Å was partitioned among the ${}^2D_{5/2}$, ${}^2D_{3/2}$, and ${}^2S_{1/2}$ channels according to the data in Table I. Then the cross section of the ${}^2S_{1/2}$ continuum was taken from the data of Brehm³⁰ immediately at the first ionization threshold, using the measurement of Lincke and Stredele to normalize Brehm's curve. The value there was 3.4 Mb and was reasonably close to the value of 3.0 ± 0.1 obtained by measurements of Berkowitz and Lifshitz, normalized in the same way. A smooth curve was constructed for the ${}^2S_{1/2}$ partial cross section, using the cross-section value at threshold, 584 and 304 Å, and recognizing that a Cooper zero is present in the $6s - \epsilon p$ cross section. This zero, caused by a change in sign of the dipole matrix element, was located at $\hbar\omega \sim 18$ eV by a Hartree-Slater calculation.

Second, the ${}^2S_{1/2}$ part of the cross section was subtracted from the total cross section, which was

then divided between the ${}^2D_{5/2}$ and ${}^2D_{3/2}$ channels according to the smooth curve in Fig. 4. The bold dots in Fig. 5 denote points for which experimental branching ratios were measured. The solid lines denote regions of high confidence resulting from interpolation among the measured branching ratios. The dashed portions represent results of reasonable extrapolation. The cross section at the ${}^2D_{5/2}$ threshold was deduced by first determining the cross section at 15.25 eV by subtracting the ${}^2S_{1/2}$ cross section from the revised total cross section of 4.75 Mb obtained from Cairns *et al.* Then a smooth curve was constructed from the known region of the spectrum above $\hbar\omega = 20$ eV through the point at 15.25 eV to set the threshold value. The cross section at the onset of the ${}^2D_{3/2}$ threshold was then obtained by subtracting the ${}^2S_{1/2}$ and ${}^2D_{5/2}$ values from the total.

It should also be pointed out that the partial cross sections at the ${}^2D_{5/2}$ and ${}^2D_{3/2}$ thresholds can be deduced by extrapolation from the discrete portion of each channel. This can be carried out using an independent-channel³¹ or coupled-channel³² procedure. Both procedures require knowledge of a sufficient number of energy levels and intensities in the autoionization region to permit smooth extrapolation into the continuum. We believe sufficient energy-level data are available from photographic measurements.³³ However, measurements reporting intensities in the autoionizing portion of the spectrum completely resolve the component terms of only the first two or three members of the series. The unresolved peaks could be partitioned between their components by assuming specified shapes for the energy dependence of the dipole matrix elements to each series of sublevels, but we have not done so here.

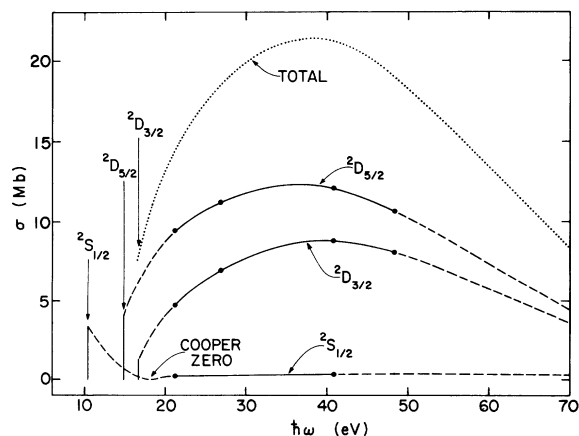


FIG. 5. Partial photoionization cross sections for Hg.

IV. DISCUSSION

The results for the ${}^2D_{5/2}$ and ${}^2D_{3/2}$ partial cross sections may now be compared with the Dirac-Slater results of Walker *et al.*² Most importantly, the experiment supports the prediction based on the calculation that the ${}^2D_{5/2}$: ${}^2D_{3/2}$ branching ratio should be larger than statistical when the partial cross sections are rising and below statistical when they are falling. Of course, statements of this type are slightly oversimplified for emphasis, and exceptions can be found. For instance, this rule will be of no help in predicting the branching ratio in the vicinity of the maxima in the partial cross sections, except that it will be passing through the statistical value near the maxima. In cases such as Hg, where the spin-orbit splitting is large, the partial cross sections for the two spin-orbit substates are not only shifted by the spin-orbit splitting, they are also distorted in shape, and the maximum cross section per electron may be different (cf. Fig. 1 of Ref. 2). Hence, the crossover need not fall midway between the two maxima. In the Dirac-Slater calculation, the crossover occurred at the maxima of the ${}^2D_{3/2}$ curve. In the experimental results it occurred at 400 Å, which is below the ${}^2D_{5/2}$ maximum. Despite this difference in detail, the experimental results do verify the predictions and related physical picture of Ref. 2.

On a more quantitative level there are significant differences between experiment and theory. The experiment,²⁵ with the normalization we have chosen, exhibits a maximum cross section of ~21.5 Mb at ~38 eV, whereas the Dirac-Slater calculation² peaks at ~27 eV with a maximum of ~55 Mb. Thus, the one-electron theory predicts a higher peak at lower photon energy. This discrepancy is largely attributable to the use of the Slater exchange approximation. In so doing, the exchange interaction between the photoelectron and the hole left behind is neglected. In situations where an $l > 0$ electron is ionized and an $l + 1$ orbital with the same principal quantum number is not fully occupied, this interaction can be very large, i.e., 5–20 eV. Including this interaction in an intrachannel coupling scheme has the effect of redistributing the oscillator strength, causing a broader maximum at somewhat higher energies. This effect has been observed in a number of calculations on $3p$ absorption in Ar,^{34–36} $5p$ absorption in Xe,^{34–37} and $4d$ absorption in the rare earths³⁸ and others.^{35, 36} Computational schemes, including Hartree-Fock,³⁶ random-phase approximation,^{35, 37} and intrachannel interactions in a Hartree-Slater basis³⁴ have documented this effect. It would be very timely to conduct similar

calculations on 5*d* photoionization in mercury. By taking spin-orbit coupling into account (i.e., by working with a Dirac-Slater basis set, for example) it should now be possible to compare such a calculation with experiment on a partial-cross-section basis instead of comparing only the total-cross-section results as was previously done.

With regard to the $^2S_{1/2}$ channel, it is interesting to note that a Cooper zero occurs in this partial cross section at about $\hbar\omega = 18$ eV, according to the

Hartree-Slater model. This zero is analogous to that observed in alkali-metal³¹ and alkaline-earth spectra,³¹ but it is obscured in the total absorption or ionization spectrum of Hg by the much larger cross section for 5*d* excitation. The presence of a Cooper minimum is implied in the experimental results by the nonmonotonic decline of the $^2S_{1/2}$ partial cross section from threshold to its values at 584 and 304 Å.

†Work performed under the auspices of the U. S. Atomic Energy Commission.

- ¹J. Berkowitz, J. L. Dehmer, Y.-K. Kim, and J. P. Desclaux, *J. Chem. Phys.* (to be published).
- ²T. E. H. Walker, J. Berkowitz, J. L. Dehmer, and J. T. Waber, *Phys. Rev. Lett.* **31**, 678 (1973).
- ³D. Liberman, J. T. Waber, and D. T. Cromer, *Phys. Rev.* **137**, 27 (1965).
- ⁴J. A. R. Samson, *Adv. At. Mol. Phys.* **2**, 177 (1966).
- ⁵J. A. R. Samson and R. B. Cairns, *Phys. Rev.* **173**, 80 (1968).
- ⁶F. J. Comes and H. G. Sälzer, *Z. Naturforsch A* **19**, 1230 (1964).
- ⁷M. O. Krause and F. Wuilleumier, *J. Phys. B* **5**, L143 (1972).
- ⁸F. Wuilleumier and M. O. Krause, *Phys. Rev. A* **10**, 242 (1974).
- ⁹V. I. Kleimenov, Yu. V. Chizhov, and F. I. Vilesov, *Opt. Spektrosk.* **32**, 702 (1971) [*Opt. Spectrosc.* **32**, 371 (1972)].
- ¹⁰J. L. Bahr, A. J. Blake, J. H. Carver, J. L. Gardner, and V. Kumar, *J. Quant. Spectrosc. Radiat. Transfer* **12**, 59 (1972).
- ¹¹J. L. Gardner and J. A. R. Samson, *J. Elect. Spectrosc.* **2**, 153 (1973).
- ¹²J. A. R. Samson and J. L. Gardner, *J. Geophys. Res.* **78**, 3663 (1973).
- ¹³J. L. Bahr, A. J. Blake, J. H. Carver, and V. Kumar, *J. Quant. Spectrosc. Radiat. Transfer* **9**, 1359 (1969).
- ¹⁴J. H. Carver and J. L. Gardner, *J. Quant. Spectrosc. Radiat. Transfer* **12**, 59 (1972).
- ¹⁵J. L. Bahr, A. J. Blake, J. H. Carver, J. L. Gardner, and V. Kumar, *J. Quant. Spectrosc. Radiat. Transfer* **11**, 1853 (1971).
- ¹⁶J. Berkowitz, *J. Chem. Phys.* **56**, 2766 (1972).
- ¹⁷R. G. Newburgh, L. Heroux, and H. E. Hinteregger, *Appl. Opt.* **1**, 733 (1962).
- ¹⁸J. L. Dehmer, J. Berkowitz, and J. C. Person, Argonne National Laboratory Radiological and Environmental Research Division Annual Report No. ANL-7960, 1971-1972, Part I, p. 88 (unpublished); J. C. Person, P. P. Nicole, and J. L. Dehmer, Argonne National Laboratory Radiological and Environmental Research Division Annual Report No. ANL-8060, 1972-1973, Part I, p. 166 (unpublished).
- ¹⁹L. J. Kieffer, *At. Data* **2**, 293 (1971).
- ²⁰F. Herman and S. Skillman, *Atomic Structure Calculations* (Prentice-Hall, Englewood Cliffs, 1963).
- ²¹J. Cooper and R. N. Zare, in *Lectures in Theoretical Physics, Vol. 11c, Atomic Collision Processes*, edited by S. Geltman, K. Mahantharpa, and W. Brittin (Gordon and Breach, New York, 1969), p. 317.
- ²²S. T. Manson, *Chem. Phys. Lett.* **19**, 76 (1973).
- ²³D. C. Frost, C. A. McDowell, and D. A. Vroom, *Chem. Phys. Lett.* **1**, 93 (1967).
- ²⁴D. C. Frost, C. A. McDowell, and D. A. Vroom, *Proc. R. Soc. A* **296**, 566 (1967).
- ²⁵R. B. Cairns, H. Harrison, and R. J. Schoen, *J. Chem. Phys.* **53**, 96 (1970).
- ²⁶R. Lincke and B. Stredle, *Z. Phys.* **238**, 164 (1970).
- ²⁷A. Skerbele, K. J. Ross, and E. N. Lassetre, *J. Chem. Phys.* **50**, 4486 (1969).
- ²⁸J. Berkowitz and C. Lifshitz, *J. Phys. B* **1**, 438 (1968).
- ²⁹J. Berkowitz (unpublished).
- ³⁰B. Brehm, *Z. Naturforsch. A* **21**, 196 (1966).
- ³¹U. Fano and J. W. Cooper, *Rev. Mod. Phys.* **40**, 441 (1968), Sec. 2.4.
- ³²K. T. Lu, *Phys. Rev. A* **4**, 579 (1971); C. M. Lee and K. T. Lu, *Phys. Rev. A* **8**, 1241 (1973).
- ³³W. R. S. Garton and J. P. Connerade, *Astrophys. J.* **155**, 667 (1969); M. W. D. Mansfield, *Astrophys. J.* **180**, 1011 (1973).
- ³⁴A. F. Starace, *Phys. Rev. A* **2**, 118 (1970).
- ³⁵M. Ya. Amusia, N. A. Cherepkov, and L. V. Chernysheva, *Zh. Eksp. Teor. Fiz.* **60**, 160 (1971) [*Sov. Phys.—JETP* **33**, 90 (1971)].
- ³⁶D. J. Kennedy and S. T. Manson, *Phys. Rev. A* **5**, 227 (1972).
- ³⁷G. Wendin, *J. Phys. B* **6**, 42 (1973), and references therein.
- ³⁸A. F. Starace, *J. Phys. B* **7**, 14 (1973), and references therein.